



Femtosecond laser 3D micromachining: a powerful tool for the fabrication of microfluidics, optofluidics, and electrofluidics based on glass

Journal:	<i>Lab on a Chip</i>
Manuscript ID:	LC-CRV-05-2014-000548.R1
Article Type:	Critical Review
Date Submitted by the Author:	10-Jun-2014
Complete List of Authors:	Sugioka, Koji; RIKEN Center for Advanced Photonics, RIKEN-SIOM Joint Research Unit Xu, Jian; RIKEN Center for Advanced Photonics, RIKEN-SIOM Joint Research Unit Wu, Dong; RIKEN Center for Advanced Photonics, Hanada, Yasutaka; Hirosaki University, Wang, Zhongke; Singapore Institute of Manufacturing Technology, Cheng, Ya; Shanghai Institute of Optics and Fine Mechanics, Midorikawa, Katsumi; RIKEN Center for Advanced Photonics,

Femtosecond laser 3D micromachining: a powerful tool for the fabrication of microfluidics, optofluidics, and electrofluidics based on glass

Koji Sugioka^{*a}, Jian Xu^a, Dong Wu^a, Yasutaka Hanada^b, Zhongke Wang^c, Ya Cheng^d, and Katsumi Midorikawa^a

^aRIKEN Center for Advanced Photonics, Wako, Saitama 351-0198, Japan, *E-mail: ksugioka@riken.jp, Fax: +81-48-462-4682, Tel: +81-48-467-9495

^bHirosaki University, Graduate School of Science and Technology, Hirosaki, Aomori 036-8561, Japan

^cSingapore Institute of Manufacturing Technology, 71 Nanyang Drive, Singapore 638075

^dShanghai Institute of Optics and Fine Mechanics, Chinese Academy of Sciences, No. 390 Qinghe Road, Jiading, Shanghai 201800, China

Femtosecond laser has unique characteristics of ultrashort pulse width and extremely high peak intensity; however, one of the most important features of femtosecond laser processing is that strong absorption can be induced only at the focus position inside transparent materials due to nonlinear multiphoton absorption. This exclusive feature makes it possible to directly fabricate three-dimensional (3D) microfluidics in glass microchips by two methods: 3D internal modification using direct femtosecond laser writing followed by chemical wet etching (femtosecond laser assisted etching; FLAE) and direct ablation of glass in water (water-assisted femtosecond laser drilling: WAFLD). Direct femtosecond laser writing also enables the integration of micromechanics, microelectronics, and microoptics into the 3D microfluidics without stacking or bonding substrates. This paper gives a comprehensive review on state-of-the-art femtosecond laser 3D micromachining for the fabrication of microfluidics, optofluidics, and electrofluidics. A new strategy (hybrid femtosecond laser processing) is also presented, in which FLAE is combined with femtosecond laser two-photon polymerization to realize a new type of biochip termed the ship-in-a-bottle biochip.

Introduction

Femtosecond laser processing opened up new avenue in materials processing due to its unique characteristics of ultrashort pulse width and extremely high peak intensity [1,2]. The ultrashort pulse width of a femtosecond laser can minimize the formation of a heat-affected zone at the processed region, which enables high-quality micro- and nanofabrication of a variety of materials [3]. In addition, its extremely high peak intensity induces nonlinear absorption process in transparent materials. When light whose photon energy exceeds the band gap of a material is incident on the material, it is absorbed and a single photon excites an electron from the valence band to the conduction band. On the other hand, light whose photon energy is smaller than the band gap cannot excite electrons, so that no absorption occurs in the stationary state. However, when an extremely high density of photons is simultaneously incident on the material, an electron can be excited by multiple photons, even when the band gap exceeds the photon energy. This nonlinear process is known as multiphoton absorption. The extremely high density of photons required to induce multiphoton absorption can be easily obtained by femtosecond lasers due to their extremely high peak intensity. Thus, the femtosecond laser also enables transparent materials to be machined with high quality [4,5]. Multiphoton absorption can be efficiently induced only at intensities above a critical value that depends on both the material and the pulse width. Therefore, if a femtosecond laser beam is focused with a moderate pulse energy inside a transparent material such as glass, then multiphoton absorption can be confined to the region near the focal point, so that internal modification and three-dimensional (3D) microfabrication of the glass can be realized [6,7]. Thus, femtosecond laser processing provides some advantages over conventional methods such as traditional semiconductor processing or soft lithography for the fabrication of microfluidic, optofluidic, and lab-on-a-chip devices. The features fabricated on devices using these traditional methods can only be fabricated on the surfaces of the substrates. Thus, subsequent bonding is often required to isolate the open features from the environment. Depending on the substrate materials involved, typical bonding techniques include fusion bonding (glass and glass) [8], anodic bonding (silicon and glass) [9], oxygen plasma bonding (polydimethylsiloxane (PDMS) and glass, and PDMS and PDMS) [10], and UV curable adhesive bonding [11]. In addition to an increase in the number of process steps, potential issues caused by these additional bonding techniques are leakage of liquid samples and clogging of the thin channels. These issues become more severe for the fabrication of 3D structures of complex multilayer configurations, because a failure in one layer will affect the performance of the entire device. In contrast, femtosecond laser micromachining can

completely eliminate the bonding procedure because 3D microfluidic structures can be directly fabricated inside glass based on multiphoton absorption. Two methods are currently employed to fabricate 3D microfluidic structures; 3D internal modification by direct femtosecond laser writing followed by chemical wet etching (femtosecond laser assisted etching; FLAE) [12,13] and direct ablation of glass in water (water-assisted femtosecond laser drilling: WAFLD) [14]. Furthermore, the capability of internal processing with a femtosecond laser allows the fabrication of micromechanics [15,16], microelectronics [17], and microoptics [18,19] in glass chips. Furthermore, these microcomponents can be easily integrated with 3D microfluidics in a single glass microchip by a simple procedure [20-22]. Biochips fabricated using femtosecond lasers have already been used for some biological studies, such as nanoaquariums to determine the functions of living microorganisms [23-25], optofluidic sensors with various functionalities to detect the concentrations of liquid samples [26,27], for the detection and manipulation of single cells [28-31], and to rapidly screen algae populations [32-34].

In this paper, we give a comprehensive review on state-of-the-art femtosecond laser 3D micromachining for the fabrication of microfluidics, optofluidics, and electrofluidics based on glass, including relevant demonstrations of the fabricated biochips for biological studies. A new strategy referred to as hybrid femtosecond laser microprocessing is also introduced, in which FLAE is combined with two-photon polymerization (TPP) to enhance the functionalities of biochips [35].

Fabrication methods of functional microcomponents

Fabrication methods of 3D hollow microstructures

FLAE involves irradiation with a tightly focused femtosecond laser beam inside glass, which can locally modify the chemical properties. Successive chemical wet etching in diluted hydrofluoric (HF) acid solution (typically 5–10%) selectively removes the laser-modified regions, which results in the formation of 3D hollow microstructures such as microfluidic structures inside glass. For this process, both photosensitive glass [13,36,37] and fused silica [12,38] are typically used. Figures 1(a)-(c) schematically show the procedures for the fabrication of 3D microfluidic structures in photosensitive glass. Thermal treatment of the photosensitive glass is required prior to chemical wet etching to develop the laser-modified regions because the process relies on photochemical reaction [23,39]. However, it is more advantageous to use photosensitive glass for the fabrication of large scale or complex microfluidic structures due to two factors. First, modification in photosensitive glass with femtosecond laser irradiation can be induced at much lower peak intensities than in fused

silica, which enables the use of higher scan speeds so that the writing time is shortened. Second, despite the comparable femtosecond laser induced etch selectivity of photosensitive glass and fused silica, the former provides a higher overall etch rate than the latter. Another advantage of photosensitive glass compared with fused silica is that smooth surfaces with optical quality can be easily fabricated by post-thermal treatment after the etching process [18,19,40]. This technique can also be extended to fabricate microoptics such as micromirrors and microlenses in photosensitive glass [18,19]. Photosensitive glass also provides a unique ability for the selective precipitation of silver nanoparticles and the growth of crystalline lithium metasilicate in the irradiated region, by which microoptical filters with arbitrary attenuation values can be easily produced [25].

In contrast, fused silica eliminates the need for thermal treatment because it is directly modified due to the physical reaction induced by the femtosecond laser. In addition to a simpler procedure, fused silica offers better optical properties that include broader transmission from the UV to near IR ranges and lower autofluorescence, which are desirable for optofluidic applications.

The etch selectivity of both photosensitive glass and fused silica by FLAE is ca. 50 using diluted HF; therefore, the fabricated microchannels inevitably have tapered angles, which induce variations in the fluid flow velocity. However, a significant enhancement of the etch selectivity has been achieved using KOH solution instead of dilute HF acid solution as the etchant, as shown in Fig. 2, although the etch rate is much lower than that of HF [41]. Figure 2 clearly shows that the channels formed using KOH have much more uniform diameters, and almost 1 cm long through channels with an aspect ratio of ca. 200 from one side to the other were successfully formed in fused silica.

Another method for the fabrication of 3D microfluidic structures in glass is WAFLD, in which a glass substrate immersed in distilled water is ablated from the rear surface by direct femtosecond laser writing, as shown in Fig. 3 [14]. In this process, the liquid has an important role to efficiently remove debris from the ablated regions, which results in the formation of long microfluidic channels with complicated structures. In contrast to FLAE, this technique can be applied to any material that is transparent to the writing pulses because it relies on ablation by multiphoton absorption of the femtosecond laser [42]. This fabrication principle can also provide better uniformity of the channel diameter. WAFLD can be used to produce very narrow channels inside glass for the same reason. Nanochannels with diameters of only ca. 700 nm and with arbitrary geometry have been fabricated in fused silica using low energy near the ablation threshold of femtosecond laser pulses tightly focused by a high-numerical-aperture (NA) objective lens [43]. However, when the drilling length

reaches several hundreds of micrometers, the debris generated by femtosecond laser ablation can still clog the microchannel, which restricts the length of the fabricated microchannels to ca. 1 mm [44,45].

To overcome this problem of WAFLD and eventually achieve fabrication of microchannels with almost unlimited lengths and arbitrary geometries, the ablation of mesoporous glass immersed in water followed by post-annealing has been demonstrated [46-48]. In this process, ablation inside porous glass immersed in distilled water is first performed by direct femtosecond laser writing. Commercially available porous glass substrates typically contain pores with a mean size of ca. 10 nm that are distributed uniformly in the glass and occupy 40% of the glass volume. The pores in porous glass form a 3D connective network, which allows liquid to flow inside the glass and results in the efficient removal of debris from the ablated regions. After ablation by direct laser writing, the sample is annealed for consolidation into a compact glass. Thereby, the pores in the glass can be completely removed while the 3D microchannels still remain formed inside the glass.

Optical waveguide writing

Optical waveguides can be written inside fused silica and photosensitive glass chips by locally altering the refractive index based on the multiphoton absorption of femtosecond lasers [6,49]. There are already several review articles available on the writing of passive and active optical waveguide devices [50-53]. When microfluidic and microoptical components made of hollow structures are integrated with optical waveguides in a device, the waveguides are always written after fabrication of the hollow structures. Neither heat treatment nor wet etching is applied to the glass sample after waveguide writing.

Space-selective metallization

Metal thin films can be space-selectively deposited on the internal wall surfaces of 3D glass microfluidics created by FLAE [17]. The selective metallization procedure involves two processes: femtosecond laser ablation to roughen the internal surfaces of the glass microchannels, and selective metallization, which involves electroless metal plating. Electroless copper plating is performed first to create seed layers for subsequent electroless gold plating, where gold plating is employed to ensure sufficient chemical stability of the deposited metal films for biochip applications. Pre-deposition of copper is necessary to enhance the adhesion strength of the deposited metal films. The electroless plating solutions are mixed with reducing agents to facilitate the reduction of the

metal ions to metal atoms during the plating process. The precipitated metal atoms cannot be deposited on a smooth glass surface due to weak adhesion, whereas they can be strongly adhered to a roughened surface due to anchor effect; therefore, the space-selective deposition of metal films can be achieved on laser-ablated regions [54]. Sidewall metallization is important in electrical wiring circuits formed in 3D microfluidics connected to an external power supply (Fig. 4(a)). Sidewall metallization of microfluidic structures has been successfully demonstrated for the first time using the volume-writing scheme as shown in Fig. 4(b) [17].

Two-photon polymerization (TPP)

TPP is widely used to fabricate functional microcomponents for biochip applications [55-57]. The TPP technique is based on the two-photon absorption of femtosecond laser pulses in a photosensitive resin, which only occurs in the central region of the focal spot where the laser intensity exceeds the TPP threshold [58,59]. Writing of pre-designed 3D micro and nanostructures is realized by conversion of a liquid resin to the solid phase, point-by-point, using a focused femtosecond laser beam. TPP is now one of the major approaches to laser-based 3D printing with nanometer-scale feature sizes. The basic concept, characteristics, range of materials, and potential applications for TPP have been previously reviewed [60-62].

TPP was combined with FLAE (hybrid femtosecond laser microprocessing) to enhance the functionalities of biochips by the integration of polymer 3D micro- and nanostructures into 3D glass microfluidics [35]. Figure 1 shows the procedure for the hybrid femtosecond laser microprocessing. 3D glass microfluidic structures fabricated by FLAE (Figs. 1(a)-(c)) are filled with an epoxy-based negative-type resin for TPP fabrication (Fig. 1(d)). Prior to TPP, the sample is pre-baked to evaporate the solvent in the resin. TPP is performed using the femtosecond laser (Fig. 1(e)). After direct femtosecond laser writing, the resin is post-baked and developed in a developer to remove the unsolidified liquid resin. This hybrid technique results in 3D polymer micro and nanostructures that are integrated into the 3D glass microfluidics (Fig. 1(f)). Such an integrated microchip has been termed a ship-in-a-bottle biochip because the polymer 3D micro- or nanostructure is created within the embedded 3D glass microfluidic structure after fabrication of the microfluidic channels, similarly to the fabrication of a real ship-in-a-bottle (Fig. 1(g)).

Fabrication of biochips

3D microfluidics and nanofluidics

Figures 5(a)-(d) show 3D microfluidic structures fabricated in photosensitive glass using FLAE [16]. X-shaped microfluidic channels connected to five open microreservoirs were embedded in photosensitive glass 300 μm below the surface. A straight microchannel with a width of 45 μm and a length of 2.8 mm was successfully fabricated. The diameter is almost unchanged over the full length of the fabricated microchannel. The cross-sectional shape of microfluidic channels can be freely designed and controlled by programming the writing scheme for direct femtosecond laser writing, which provides a more biomimetic environment for cell culture and many other applications. Figure 5(e) shows scanning electron microscope (SEM) images of fabricated microchannels with rectangular, round, elliptical, pentagrammatic, triangular, and pentagonal cross-sections [35].

One of the interesting applications of 3D microfluidics fabricated by FLAE is the dynamic observation of microorganisms. *Euglena gracilis* is a single-celled organism that lives in fresh water and has a flagellum at its anterior end, which it whips rapidly to swim in water. Many biologists have used optical microscopy to investigate the continuous movement of the flagellum in relation to biomotor applications in biology, and ultimately to determine the origin of this functionality. However, only the thrusting movement of the flagellum has been investigated [63,64], and the detailed mechanism is still unknown due to the difficulties in capturing images of the rapid continuous movement of the flagellum. To clearly and efficiently observe flagellum movement, a simple microfluidic channel with a rectangular cross-section embedded in photosensitive glass was fabricated by FLAE, a schematic illustration of which is shown in Fig. 6(a) [24]. The rectangular cross-section microfluidic channel has flat and smooth internal walls, which is essential to capture clear images of *Euglena gracilis* swimming in the microchannel using a microscope. *Euglena gracilis* is confined to a limited volume in the microchannel, which enables the flagellum movement to be easily observed using a microscope. Such a microfluidics reduces the observation time by a factor greater than 10 compared to conventional methods using a Petri dish when observed from position (1) in Fig. 6(a). Furthermore, observations from position (2) enabled a front view of *Euglena gracilis* to be obtained, as shown in Fig. 6(b). This is the first time that such an image has been obtained, and thereby 3D analysis of flagellum movement that results in propulsion has been realized. Biochips used for the dynamic observation and determination of microorganism functions have been termed nanoaquariums [24,25].

Another application of 3D microfluidics fabricated by FLAE is cell sorting. Populations of cells often involve some heterogeneity that can cause problems in experiments to examine cellular biology. It is important to retrieve species of interest from a heterogeneous mass for biological

studies such as culturing, genetic analysis, etc. For example, a 3D mammalian cell separator biochip was fabricated in fused silica by FLAE [65]. Cell sorting relies on differences in deformability due to dissimilar cytoskeletal architecture in diverse cell types. Figure 7(a) illustrates the principle of a biochip fabricated for cell sorting, which consists of a T-junction formed by two microchannels connected with narrow constrictions. These constrictions function as filters for sorting. The structure enables accurate pressure-driven flow control, which results in the deformation of cells according to their specific characteristics. When a heterogeneous population of cells is introduced into such a biochip from the inlet, the softer cells are deformed by a pressure gradient maintained across the constrictions and then guided through the constrictions into outlet 1 of the device. The cross-section of the constrictions should be narrower than the average size of the cells. Thus, more rigid cells are not sufficiently deformed to pass through the constrictions and instead flow to the direction of outlet 2. For demonstration of the fabricated cell separator biochip, a T-junction device with 18 constrictions, as shown in Fig. 7(b), was employed. Human promyelocytic leukemia (HL60) cells were injected into the left-side microfluidic channel at a constant flow rate of 0.5 mL/min. The average size of healthy looking cells was measured as $11.7 \pm 1.1 \mu\text{m}$ with a standard deviation of 1.09 for 25 cells, while the cross-section of the constriction was $4 \times 8 \mu\text{m}^2$ with a length of 200 μm . The HL60 cells were successfully collected in the right-side microfluidic channel passing through the constriction with 81% of the collected cells viable. This result indicated that a heterogeneous population of cells could be successfully separated based on the differences in the deformability of each cell.

Apart from microfluidic channels, this technique can be extended to fabricate fluid control microcomponents, such as microvalves and micropumps, for microfluidic devices [15,16,66]. Figure 8 shows a 3D schematic illustration with overview and close-up optical micrographs of a micropump integrated into a microfluidic structure. In this structure, a cross-shape microcomponent connected with a rod was fabricated in a hollow microfluidic chamber embedded in photosensitive glass. The microcomponent is free from the glass substrate, so that it is freely movable in the microfluidic chamber. Connection of the hole formed in the rod with an external DC micromotor allows the microcomponent to be rotated and act as a micropump. This micropump can control the flow velocity of water up to ca. 800 $\mu\text{m/s}$, which corresponds to a flow rate of ca. 50 mm^3/s , by changing the rotation speed.

WAFLD can be used to fabricate more complicated structures because it does not rely on an enhanced etching rate in HF solution. The multilayered microfluidic system with 3D configuration

shown in Fig. 9 was constructed in fused silica using WAFLD [67]. Microfluidic channels with helical structures were formed at three layers of 300, 500, and 700 μm beneath the glass surface. This microfluidic system can be used with four different liquids that are injected from each inlet (A–D) and two specific liquids can be mixed in any of the microchannels (1–5). For example, liquids injected from inlets C and D are mixed in microchannel 5 and the mixed liquids are discharged from outlet 5. In this way, the five different combinations of liquid mixing can be achieved simultaneously.

WAFLD treatment of porous glass was used to fabricate sub-50 nm nanofluidics channels by combining the threshold effect and the formation of a periodic nanograting. A nanoscale periodic grating is formed inside the glass when irradiated with a linearly polarized beam [68], because the energy deposition inside the glass is spatially modulated with nanoscale periodicity at the focal spot, as shown in Fig. 10(a). When the femtosecond laser intensity is intentionally reduced to a level at which only the intensity in the blue region of Fig. 10(a) exceeds the threshold intensity, only a single cycle of the modulated energy distribution in the central area of the focal volume can be selected. It is noteworthy that the peak laser intensity at the center of the focal spot is still much greater than the laser intensity at the edge of the blue zone (i.e., the threshold intensity). Using this scheme, Fig. 10(b) shows a nanochannel with a width of ca. 40 nm and a length of ca. 40 μm (aspect ratio of ca. 1,000) that was fabricated by the ablation of porous glass in water using a linearly polarized femtosecond laser beam [69]. Such nanofluidic systems have been used for DNA analysis, such as the stretching of DNA molecules.

Optofluidics

The intrinsic properties of glass in the unexposed region do not change significantly, even after multiple thermal treatments; therefore, optical waveguides can be written inside the glass by femtosecond laser-induced refractive index modification after FLAE. Thus, the 3D integration of waveguides with microfluidics can be realized in a single glass chip for the fabrication of optofluidics. The most typical optofluidics fabricated by direct femtosecond laser writing consist of optical waveguides that intersect the microfluidic channel at a right angle. This type of optofluidic device has been used to measure the concentrations of liquid samples [26,27], for the detection and manipulation of single cells [28-31], and for the rapid screening of algae populations [32-34].

Cell sorting using this type of optofluidic system involves utilizing optical forces combined with fluorescence detection of the cells [31]. Figure 11(a) illustrates the principle of cell sorting using this

scheme. Two input channels (INs) are merged into a single straight channel where fluorescence detection and sorting are conducted to separate the cells into two output channels (OUTs). The sample liquid containing cells and a buffer solution are introduced into IN1 and IN2, respectively. Appropriate control of the fluid flow rates induces laminar flow in the single straight channel, so that the entire sample with cells is exhausted to OUT1. The application of optical forces pushes cells into the buffer solution side, where the cells are collected in OUT2. Sorting can be automatically performed based on the fluorescence detection of cells, where a fluorescence laser beam is directed by a fluorescence waveguide (FWG) to the microchannel, which illuminates the entire height of microchannel to detect all cells flowing in the microchannel. In this case, the power of the fluorescence laser beam is sufficiently low to exert no optical force on the cells. The specific fluorescence signal can be detected when the target cells pass through a region in front of the FWG. Detection of the fluorescence signal automatically switches on the optical force laser beam, which is guided to the microchannel by the sorting waveguide (SWG), after a moderate delay time to synchronize with the passage of the detected cells in front of the SWG. The target cells are then pushed into the buffer solution side and eventually sorted to OUT2. A cell sample that consisted of transformed human fibroblasts transfected by plasmid encoding with an enhanced green fluorescent protein (EGFP; excitation $\lambda = 488$ nm, emission $\lambda = 505$ nm) was used for the sorting test. Approximately 50% of these cells yielded an intense green fluorescence. To excite EGFP fluorescence, a 473 nm laser was coupled into the FWG. When a non-fluorescent cell was illuminated by the FWG, it did not emit a fluorescence signal. The optical force laser beam was kept switched off and the cells continued to flow and be exhausted at OUT1 (Fig. 11(b)). In contrast, when a fluorescent cell was illuminated, a fluorescence signal was detected. After an appropriate delay time, the 1070 nm wavelength of the optical force laser beam was switched on to push the cell into the buffer solution side to sort and exhaust to OUT2, as shown in Fig. 11(c).

Another scheme for an optofluidic system involved the refractive index sensing of liquid samples based on an evanescent wave [70]. To ensure efficient overlap of the liquid sample and the evanescent wave, two microfluidic channels were fabricated in the vicinity of a Bragg grating waveguide (BGW), where the distance between the wall of microchannels and the waveguide was less than ca. 2 μm (Fig. 12(a)). The arrangement of double channels increases the amount of evanescent field that penetrates into the microfluidic channels and thus improves the device sensitivity. Detection of the refractive index change in the liquid sample can be achieved by monitoring the shift of the BGW resonances at a specific wavelength (1560 nm), as shown in Fig.

12(b). The device is capable of resolving refractive index change on the order of 10^{-4} . Further enhancement of the performance can be achieved either by promoting the quality factor of the Bragg grating cavity or by increasing the overlap area between the evanescent wave and the liquid samples (e.g., wrapping the BGW with the microfluidic channel wall).

The excellent surface smoothness of hollow structures fabricated by the FLAE of photosensitive glass has enabled further integration of microoptical components, such as micromirrors and microlenses, into optofluidic systems [18,19,40,49]. A microfluidics system with one optical waveguide and two microlenses was fabricated as an optofluidics system for photonic biosensing [40]. Figure 13(a) shows 2D and 3D schematic illustrations of the integrated optofluidics device, wherein one waveguide is connected to a microfluidic chamber, and on microlenses is arranged at the left side (in the figure) for fluorescence measurement, and at another across the microchamber at the opposite side of the optical waveguide for absorption measurement. An optical micrograph of the fabricated microchip is shown in Fig. 13(b). The fabricated optofluidics system has high sensitivity for the analysis of liquid samples based on fluorescence and absorption measurements. Figure 13(c) shows fluorescence spectra from 0.02 mol/L Rhodamine 6G (Rh6G) in the microfluidic chamber induced by a pump laser beam of 2ω from a Nd:YAG laser that was directed using the integrated optical waveguide. The fluorescence intensity was enhanced by a factor of 8 when the microlens was integrated, compared with that for a microfluidic chamber with only a waveguide and no microlens.

Another interesting feature of photosensitive glass is the ability to form optical filters, which are used to control the optical transmission of visible light, by direct femtosecond laser writing followed by thermal treatment due to the growth of a crystalline phase at the laser exposed regions. Optofluidics (nanoaquariums) integrated with optical filters have been employed to elucidate the gliding mechanism of *Phormidium*. *Phormidium* is a soil-dwelling unicellular, colonial cyanobacterium that has significant applications in agriculture because it accelerates the growth of vegetables by gliding to the seedling roots in soil [25].

Several review articles on the fabrication of optofluidics by femtosecond laser 3D micromachining are available [20-22].

Electrofluidics

Femtosecond laser ablation followed by electroless metal plating enables flexible deposition of patterned metal films on desired locations, top and bottom walls and also the sidewalls, of

microfluidic structures formed in photosensitive glass by FLAE, which is used to fabricate microfluidics integrated with microelectric devices (electrofluidics) [17]. To demonstrate the electrical functionality of conductive metal microstructures connected from the inside to the outside of a microfluidic device, a microheater was fabricated. The temperature increase with the microheater can easily exceed 200 °C, which is sufficiently high for many biochip applications. The microheater in a microfluidics system can be used as a microreactor to accelerate a chemical reaction.

Another interesting application of electrofluidics is the manipulation of biological samples. Manipulation of biological samples such as microorganisms and cells is important for many biochip applications, such as detailed observation of microorganism dynamics and tissue engineering [71,72]. Microorganisms and cells can be oriented by application of an alternating current (AC) electric field due to the interaction between the dipole moment of the target sample induced by the electric field and the electric field itself [73-75]. To realize manipulation in a microfluidic channel, an electrofluidics system that includes a microfluidic channel with a pair of integrated microelectrodes was fabricated, as schematically shown in Fig. 14(a). The optical micrograph in Fig. 14(b) shows black areas that correspond to the electrodes. *Euglena gracilis* was introduced into the microfluidic channel with water as a biosample for manipulation. Figure 14(c) shows the *Euglena* cells randomly swimming in the microchannel when no electric field is applied. As soon as an appropriate electric field is produced between the two electrodes, the movement of the *Euglena* cells is significantly changed. The bodies are rotated to orient along the electrical field lines (Fig. 14(d)). When the electric field is turned off, the movement of the microorganisms returns to the random state again (not shown in the figure).

Ship-in-a-bottle biochip

Hybrid femtosecond laser processing with FLAE followed by TPP can further enhance the functionalities of biochips. Biochips fabricated by this hybrid technique are termed ship-in-a-bottle biochips [35]. The mixing of different types of fluids is a key function for microfluidic applications [76]. To achieve efficient mixing of fluids, a polymer microcomponent fabricated by TPP (Fig. 15 (a)) was integrated into a Y-shaped microfluidic channel embedded in photosensitive glass by FLAE (Fig. 15(b)). Two different fluids (water and Rhodamine B) were poured into and effectively mixed in a short length (a few hundred micrometers) in the microfluidic channel integrated with the microdevice (Fig. 15(b)), whereas no mixing occurred and laminar flow was produced in a simple

microfluidic channel without the microdevice (Fig. 15(c)). This ship-in-a-bottle biochip was successfully applied as a microreactor for the synthesis of ZnO flower-like microparticles. This technique can also integrate microoptics such as microlenses, which will be beneficial for optofluidic applications.

Conclusions and outlook

Two direct techniques for the fabrication of 3D microfluidic structures inside glass microchips have been described; direct femtosecond laser writing followed by chemical wet etching (FLAE), and water-assisted femtosecond laser drilling (WAFLD). Both techniques can be used to fabricate hollow microstructures with almost any 3D geometry. The former technique permits microfluidic systems to be integrated with fluid control components (e.g., valves and pumps) and microoptical components (e.g., mirrors and lenses) in a single glass chip using a single continuous process. Furthermore, other microoptical components such as optical waveguides and filters, and microelectric components can be integrated by additional direct femtosecond laser writing. These techniques have been demonstrated to be very useful for the fabrication of functional biochips for biological and chemical studies that include the analysis of liquid samples, sensing, sorting, and manipulation of living cells, identification, dynamic observation and determination of microorganism functions, and the enhancement of chemical reactions. To further enhance the functionalities of fabricated biochips, a new strategy has been proposed, in which FLAE is combined with TPP (hybrid femtosecond laser microprocessing). Ship-in-a-bottle biochips fabricated using this hybrid technique exhibit high functionality.

Femtosecond laser 3D micromachining can completely eliminate the substrate stacking and bonding procedure to fabricate 3D microfluidic structures even with the multilayered geometry inside glass. Some functional microcomponents can be fabricated at the same time by a single continuous procedure. Furthermore, microelectric components and polymer microcomponents can be flexibly integrated after fabrication of 3D microfluidics by the ship-in-a-bottle fabrication scheme, which enables us to further enhance functionalities of biochips. These are definitive advantages over the conventional techniques such as PDMS-based soft lithography and traditional semiconductor processing. The soft lithography is the most widely used technique for fabrication of biochips due to its low cost, high throughput, high fabrication resolution, simplicity, and convenience. To prevail over the conventional methods, there is still room for improvement of femtosecond laser 3D

micromachining. First, the current fabrication resolution for internal 3D modification in glass is on the wavelength scale or larger, mainly due to the diffraction limit of the focusing system, the heat diffusion in the laser affected zone, and the resolution degradation in the post-exposure fabrication processes, e. g., chemical wet etching. For cutting edge fluidic and photonic applications such as nanofluidics and nanophotonics, such resolution is far from sufficient. WAFLD treatment of porous glass combined with the threshold effect and the formation of a periodic nanograting showed possibility of fabricating nanofluidics channels. Second, with either FLAE or WAFLD, the length of the microfluidic structures directly fabricated in glass is limited to a few millimeters to ~1 centimeter. In contrast, with conventional biochip fabrication techniques, there is in principle no limit on the sizes of the microfluidic chips. Fortunately, this bottleneck can be resolved by WAFLD of a porous glass. But smoothness of internal walls of fabricated microfluidics channels is insufficient for some biochip applications. It has not yet been succeeded in smoothing the surface by post thermal treatment unlike the case of FLAE of photosensitive glass. Third, substrates that can be used for biochip fabrication by femtosecond 3D laser micromachining are limited to only glass until now. Very recently, it has been preliminary demonstrated that 3D microfluidic structure can be created in fluoropolymer CYROP by FLAE [77], which will expand capabilities of FLAE. Lastly, femtosecond laser processing has long been regarded as an expensive and time-consuming technique; this image has hampered the widespread use of this technique. However, this situation is currently undergoing a change due to the development of new generation femtosecond lasers that offer higher fabrication efficiencies and operating stabilities at reduced costs [78].

On the application exploration side, femtosecond laser processing is currently not as popular as conventional techniques for biochip applications, despite its unparalleled capabilities of 3D fabrication and integration. In addition, most functional biochips produced by femtosecond laser processing involve straightforward incorporation of optical functions in microfluidic systems to enhance their sensing capabilities. Many new directions remain unexplored. For example, fabrication of tunable optical systems by synergetically combining fluidic and optical components has been intensively investigated since the birth of optofluidics [79,80]. Using femtosecond laser processing, such integrated devices can be directly fabricated in glass without post-assembling. The use of glass substrates has the potential to realize superior optical performance and chemical stability than polymers. Another fascinating opportunity is provided by the emerging optofluidic technique for sunlight-based energy applications, where optical waveguides can be incorporated into photobioreactor or photocatalytic systems to improve either the sunlight collection or distribution

performance [81]. Femtosecond laser processing is attractive due to its ability to realize one-step integration of microfluidics and micro-optical components in glasses. The selective metallization technique can also be used to produce optofluidic systems with high sensing performances based on surface-enhanced Raman scattering. Glass is an ideal substrate material for such applications mainly because of its high chemical inertness. The ultimate dream of femtosecond laser 3D micromachining is probably to create a complete “all-in-one” biochips with a multilayered geometry in which all the necessary functional components are simultaneously integrated by a single continuous procedure based on femtosecond laser direct writing followed by ship-in-a-bottle fabrication using the same laser writing system. This is certainly a formidable challenge, but significant progress has been made toward realizing this goal and important technical advances have been realized as described in this paper.

References

1. *Ultrafast laser processing: from micro- to nanoscale*, ed. K. Sugioka and Y. Cheng, Pan Stanford Publishing Pte. Ltd, Singapore, 2013, pp. 1-597.
2. K. Sugioka and Y. Cheng, *Light: Sci. & Appl.*, 2014, **3**, e149.
3. C. Momma, B. N. Chichkov, S. Nolte, F. Alvensleben, A. Tünnermann, H. Welling, and B. Wellegehausen, *Opt. Commun.*, 1996, **129**, 134-142.
4. S. Küper and M. Stuke, *Appl. Phys. Lett.*, 1989, **54**, 4-6.
5. S. Küper and M. Stuke, *Microelectron. Eng.*, 1989, **9**, 475-480.
6. K. M. Davis, K. Miura, N. Sugimoto, and K. Hirao, *Opt. Lett.*, 1996, **21**, 1729-1731.
7. E. N. Glezer, M. Milosavljevic, L. Huang, R. J. Finlay, T. H. Her, J. P. Callan, and E. Mazur, *Opt. Lett.*, 1996, **21**, 2023-2025.
8. K. M. Delft, J. C. T. Eijkel, D. Mijatovic, T. S. Druzhinina, H. Rathgen, N. R. Tas, A. van den Berg, and F. Mugele, *Nano Lett.*, 2007, **7**, 345-350.
9. N. F. Y. Durand NFY and P. Renaud, *Lab Chip*, 2009, **9**, 319-324.
10. M. A. Eddings, M. A. Johnson, and B. K. Gale, *J. Micromech. Microeng.*, 2008, **18**, 067001-067004.
11. Z. Huang, J. C. Sanders, C. Dunsmor, H. Ahmadzadeh, and J. P. Landers, *Electrophoresis*, 2001, **22**, 3924-3929.
12. A. Marcinkevicius, S. Juodkazis, M. Watanabe, M. Miwa, S. Matsuo, H. Misawa, and J. Nishii, *Opt. Lett.*, 2001, **26**, 277-279.
13. M. Masuda, K. Sugioka, Y. Cheng, N. Aoki, M. Kawachi, K. Shihoyama, K. Toyoda, H. Helvajian, and K. Midorikawa, *Appl. Phys.*, 2003, **A76**, 857-860.
14. Y. Li, K. Itoh, W. Watanabe, K. Yamada, D. Kuroda, J. Nishii, Y. Y. Jiang, *Opt. Lett.*, 2001, **26**, 1921-1924
15. M. Masuda, K. Sugioka, Y. Cheng, T. Hongo, K. Shihoyama, H. Takai, I. Miyamoto, and K.

- Midorikawa, *Appl. Phys.*, 2004, **A78**, 1029-1032.
16. K. Sugioka and Y. Cheng, *Appl. Phys. A.*, 2014, **114**, 215-221.
 17. J. Xu, D. Wu, Y. Hanada, C. Chen, S. Wu, Y. Cheng, K. Sugioka, and K. Midorikawa, *Lab Chip*, 2013, **13**, 4608-4616.
 18. Z. Wang, K. Sugioka, and K. Midorikawa, *Appl. Phys.*, 2007, **A89**, 951-955.
 19. Y. Cheng, K. Sugioka, K. Midorikawa, M. Masuda, K. Toyoda, M. Kawachi, and K. Shihoyama, *Opt. Lett.*, 2003, **28**, 1144-1146.
 20. K. Sugioka, and Y. Cheng, *MRS Bull.*, 2011, **36**, 1020-1027.
 21. K. Sugioka, and Y. Cheng, *Lab Chip*, 2012, **12**, 3576-3589.
 22. K. Sugioka, and Y. Cheng, *Femtosecond laser 3D micromachining for microfluidic and optofluidic applications*, Springer, Heidelberg, 2012, pp.1-129.
 23. K. Sugioka, Y. Hanada, and K. Midorikawa, *Laser & Photon. Rev.*, 2010, **4**, 386-400.
 24. Y. Hanada, K. Sugioka, H. Kawano, I. S. Ishikawa, A. Miyawaki, and K. Midorikawa, *Biomed. Microdevices*, 2008, **10**, 403-410.
 25. Y. Hanada, K. Sugioka, I. S.-Ishikawa, H. Kawano, A. Miyawaki, and K. Midorikawa, *Lab Chip*, 2011, **11**, 2109-2115.
 26. A. Crespi, Y. Gu, B. Ngamsom, H. J. W. M. Hoekstra, C. Dongre, M. Pollnau, R. Ramponi, H. H. van den Vlekert, P. Watts, G. Cerullo, and R. Osellame, *Lab Chip*, 2010, **10**, 1167-1173.
 27. Y. Hanada, K. Sugioka, and K. Midorikawa, *Lab Chip*, 2012, **12**, 3688-3693.
 28. M. Kim, D. J. Hwang, H. Jeon, K. Hiromatsu, and C. P. Grigoropoulos, *Lab Chip*, 2009, **9**, 311-318.
 29. N. Bellini, K. C. Vishnubhatla, F. Bragheri, L. Ferrara, P. Minzioni, R. Ramponi, I. Cristiani, and R. Osellame, *Opt. Express*, 2010, **18**, 4679-4688.
 30. F. Bragheri, L. Ferrara, N. Bellini, K. C. Vishnubhatla, P. Minzioni, R. Ramponi, R. Osellame, and I. Cristiani, *J. Biophotonics*, 2010, **3**, 234-243.

31. F. Bragheri, P. Minzioni, R. M. Vazquez, N. Bellini, P. Paie, C. Mondello, R. Ramponi, I. Cristiani, and R. Osellame, *Lab Chip*, 2012, **12**, 3779-3784.
32. A. Schaap, Y. Bellouard, and T. Rohrlack, *Biomed. Opt. Express*, 2011, **2**, 658-664.
33. A. Schaap, T. Rohrlack, and Y. Bellouard, *Lab Chip*, 2012, **12**, 1527-1532.
34. A. Schaap, T. Rohrlack, and Y. Bellouard, *J. Biophotonics*, 2012, **5**, 661-672.
35. D. Wu, S. Wu, J. Xu, L. G. Niu, K. Sugioka, and K. Midorikawa, *Laser & Photon. Rev.*, 2014, **8**, 458-467.
36. K. Sugioka, Y. Cheng, and K. Midorikawa, *Appl. Phys. A*, 2005, **81**, 1-10.
37. Y. Kondo, J. R. Qiu, T. Mitsuyu, K. Hirao and T. Yoko, *Jpn. J. Appl. Phys.*, 1999, **38**, L1146-L1148.
38. Y. Bellouard, A. Said, M. Dugan and P. Bado, *Opt. Express*, 2004, **12**, 2120-2129.
39. T. Hongo, K. Sugioka, H. Niino, Y. Cheng, M. Masuda, I. Miyamoto, H. Takai, and K. Midorikawa, *J. Appl. Phys.*, 2005, **97**, 063517.
40. Z. Wang, K. Sugioka, and K. Midorikawa, *Appl. Phys. A*, 2008, **93**, 225-229.
41. S. Kiyama, S. Matsuo, S. Hashimoto, and Y. Morihira, *J. Phys. Cem C*. 2009, **113**, 11560-11566.
42. T. N. Kim, K. Campbell, A. Groisman, D. Kleinfeld, and C. B. Schaffer, *Appl. Phys. Lett.*, 2005, **86**, 201106.
43. K. Ke, E. F. Hasselbrink, and A. Hunt, *Annal. Chem.*, 2005, **77**, 5083-5088.
44. R. An, Y. Li, Y. P. Dou, H. Yang, and Q. H. Gong, *Opt. Express*, 2005, **13**, 1855-1859.
45. D. J. Hwang, T. Y. Choi, and C. P. Grigoropoulos, *Appl. Phys. A*, 2004, **79**, 605-612.
46. Y. Liao, Y. Ju, L. Zhang, F. He, Q. Zhang, Y. Shen, D. Chen, Y. Cheng, Z. Xu, K. Sugioka, and K. Midorikawa, *Opt. Lett.* 2010, **35**, 3225-3227.
47. Y. Liao, J. Song, E. Li, Y. Luo, Y. Shen, D. Chen, Y. Cheng, Z. Xu, K. Sugioka, and K. Midorikawa, *Lab Chip* 2012, **12**, 746-749.

48. C. N. Liu, Y. Lia, F. He, J. X. Song, D. Lin, Y. Cheng, K. Sugioka, and K. Midorikawa, J. *Laser Micro/Nanoengin.* 2013, **8**, 170-174.
49. Z. Wang, K. Sugioka, Y. Hanada, and K. Midorikawa, *Appl. Phys. A*, 2007, **88**, 699-704.
50. R. R. Gattass and E. Mazur, *Nature Photon.*, 2008, **2**, 219-225.
51. K. Itoh K, W. Watanabe, S. Nolte S, and C. B. Schaffer, *MRS Bull.*, 2006, **31**, 620-625.
52. *Femtosecond laser micromachining*, ed.R. Osellame, G. Cerullo, and R. Ramponi, Springer-Verlag GmbH, Heidelberg, 2012, pp. 1-483.
53. N. Bellini, A. Cresoi, S. M. Eaton, and R. Osellame, *3D Photonic Device Fabrication* (Chap. 9 in *Ultrafast laser processing: from micro- to nanoscale*, ed. K. Sugioka and Y. Cheng, Pan Stanford Publishing Pte. Ltd, Singapore) 2013, pp. 427-488.
54. Y. Hanada, K. Sugioka and K. Midorikawa, *Appl. Phys. A*, 2008, **90**, 603-607.
55. J. Wang, Y. He, H. Xia, L. G. Niu, R. Zhang, Q. D. Chen, Y. L. Zhang, Y. F. Li, S. J. Zeng, J. H. Qin, B. C. Lin, and H. B. Sun, *Lab Chip*, 2010, **10**, 1993-1996.
56. T. W. Lim, Y. Son, Y. J. Jeong, D. Y. Yang, H. J. Kong, K. S. Lee, and D. P. Kim, *Lab Chip*, 2011, **11**, 100-103.
57. S. Maruo and H. Inoue, *Appl. Phys. Lett.*, 2007, **91**, 084101.
58. S. Maruo, O. Nakamura, and S. Kawata, *Opt. Lett.* 1997, **22**, 132-134.
59. S. Kawata, H. B. Sun, T. Tanaka, and K. Takada, *Nature*, 2001, **412**, 697-698.
60. B. B. Xu, Y. L. Zhang, H. Xia, W, F. Dong, H. Ding H, and H. B. Sun, *Lab Chip* 2013, **13**, 1677-1690.
61. S. Maruo S and J. T. Fourkas, *Laser Photonics Rev.*, 2008, **2**, 100-111.
62. D. Wu, X. F. Lin, Q. D. Cheg, H. Xia, Y. L. Zhang, and H. B. Sun, *Fabrication of 3D functional microdevices by two-photon photopolymerization* (Chap. 11 in *Ultrafast laser processing: from micro- to nanoscale*, ed. K. Sugioka and Y. Cheng, Pan Stanford Publishing Pte. Ltd, Singapore) 2013, pp. 520-568.

63. K. M. Nichols, R. Rikmenspoel, *J. Cell Sci.*, 1977, **23**, 211-225.
64. K. M. Nichols, R. Rikmenspoel, *J. Cell Sci.*, 1978, **29**, 233-247.
65. D. Choudhury, W. T. Ramsay, R. Kiss, N. A. Willoughby, L. Paterson, and A. K. Kar, *Lab Chip*, 2012, **12**, 948-953.
66. S. Kiyama, T. Tomita, S. Matsuo, and S. Hashimoto, *J. Laser Micro/Nanoengin.* 2009, **4**, 18-21.
67. Y. Li and S. Qu, *Current Appl. Phys.*, 2013, **13**, 1292-1295.
68. Y. Shimotsuma, P. G. Kazansky, J. R. Qiu, and K. Hirao, *Phys. Rev. Lett.*, 2003, **91**, 247405.
69. Y. Liao, Y. Cheng, C. Liu, J. Song, F. Hei, Y. Shen, D. Chen, Z. Xu, Z. Fan, X. Wei, K. Sugioka, and K. Midorikawa, *Lab Chip*, 2013, **13**, 1626-1631.
70. V. Maselli, J. R. Grenier, S. Ho and P. R. Herman, *Opt. Express*, 2009, **17**, 11719-11729.
71. M. Yang and X. Zhang. *Sensors Actuators A*, 2007, **35**, 73-79.
72. R. D. Miller and T. B. Jones, *Biophys. J.*, 1993, **64**, 1588-1595.
73. J. W. Choi, S. Rosset, M. Niklaus, J. R. Adleman, H. Shea and D. Psaltis, *Lab Chip*, 2010, **10**, 783-788.
74. J. L. Griffin and R. E. Stowell, *Exp. Cell Res.*, 1966, **44**, 684-688.
75. C. Ascoli, M. Barbi, C. Frediani and D. Petracchi. *Biophys. J.*, 1978, **24**, 601-612.
76. S. Jeon, V. Malyarchuk, J. O. White, and J. A. Rogers, *Nano Lett.*, **5**, 2005, 1351-1356.
77. R. Okikawa, Y. Hanada, K. Sugioka, and K. Midorikawa, *LPM 2014*, 2014, Fr2-O-2.
78. A. Tuennermann, T. Schreiber, and J. Limpert, *Appl. Opt.*, 2010, **49**, F71-F78.
79. D. Psaltis, S. R. Quake, and C. Yang, *Nature*, 2006, **442**, 381-386.
80. C. Monat, P. Domachuk, B. J. Eggleton, *Nat. Photonics*, 2007, **1**, 106-114.
81. D. Erickson, D. Sinton, and D. Psaltis, *Nat. Photonics*, 2011, **5**, 583-590.

Figures

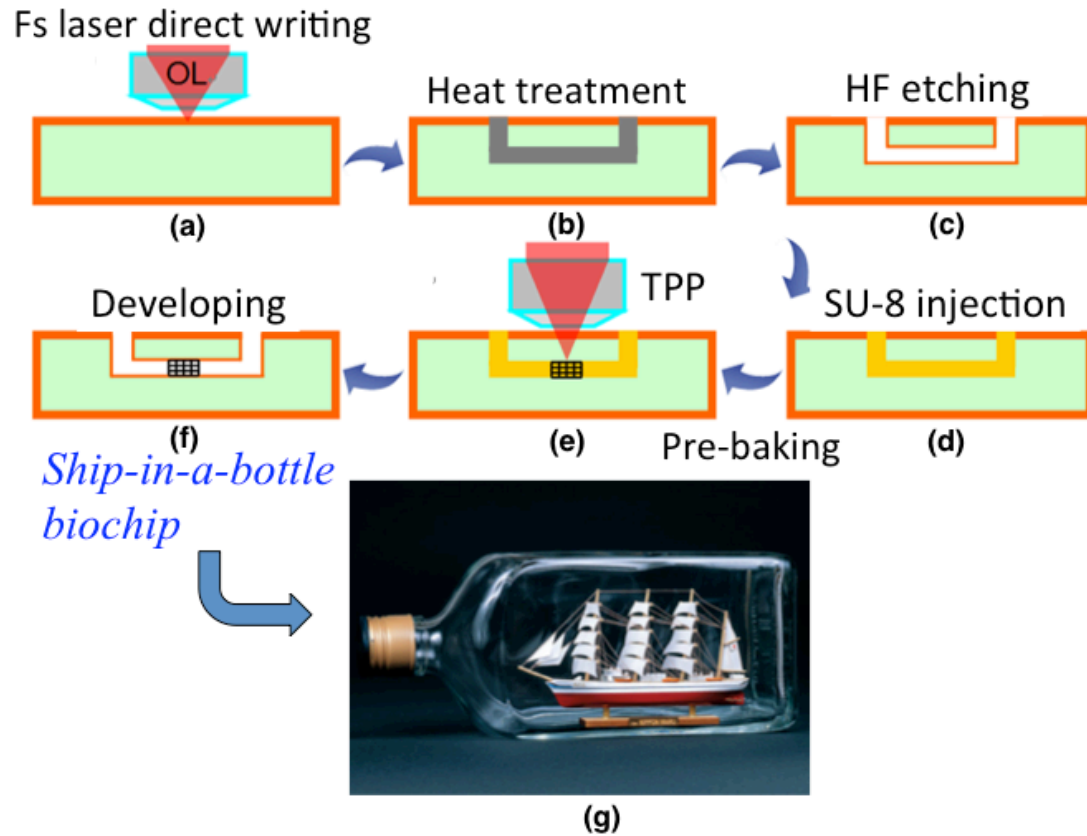


Fig. 1. Schematic illustration of fabrication procedure for a 3D ship-in-a-bottle biochip by hybrid femtosecond laser microprocessing. (a-c) FLAE of photosensitive glass, which involves (a) direct femtosecond laser writing followed by (b) heat treatment, and (c) successive HF etching. (d-f) TPP involves (d) SU-8 injection into the fabricated glass microfluidic structure, (e) direct femtosecond laser writing for TPP after pre-baking, and (f) development to form the ship-in-a-bottle biochip. A photograph of a real ship-in-a-bottle is shown in (g) for reference (courtesy of WOODYJOE Co., Ltd.).



Fig. 2. Almost 1 cm long trough channels with an aspect ratio of ca. 200 fabricated from one side to the other in fused silica by FLAE using 10 M (35.8%) aqueous KOH (20 mL) [41]. (Reproduced with permission from ACS. ©2009 by the American Chemistry Society.)

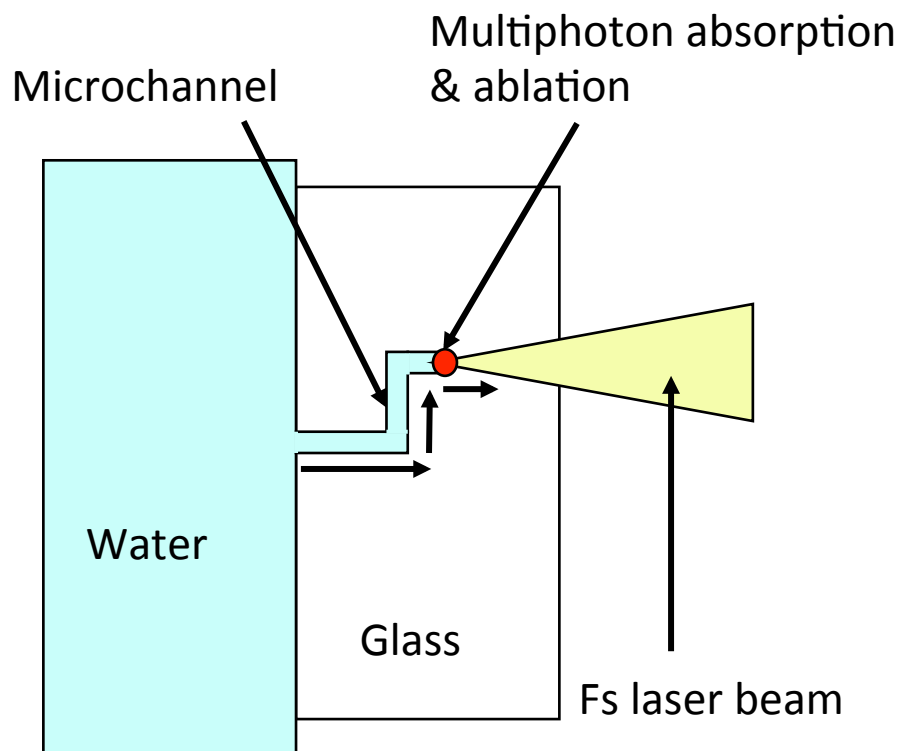


Fig. 3. Schematic diagram of water-assisted femtosecond laser drilling for the fabrication of 3D microchannels in glass.

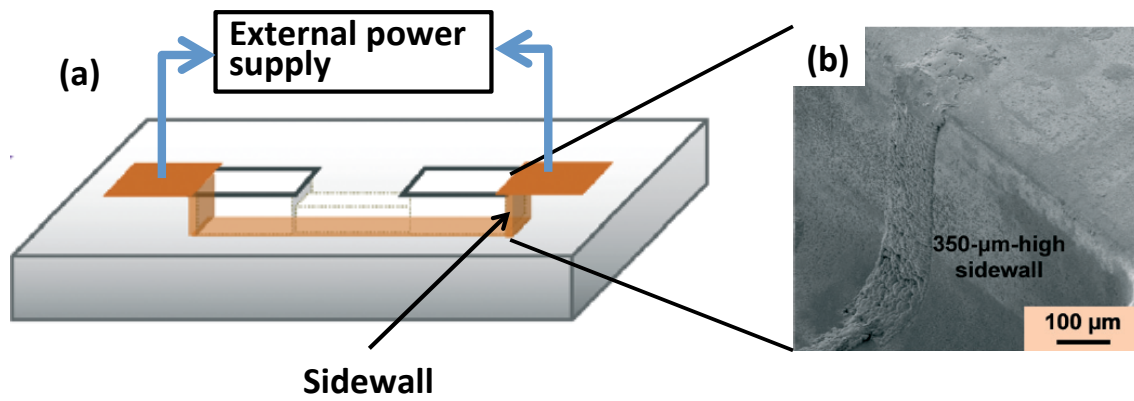


Fig. 4. (a) Schematic of electrical wiring circuits formed in 3D microfluidics connected to an external power supply. (b) 45° tilted SEM image of the metal structures formed on a 350 μm high sidewall by femtosecond laser ablation followed by electroless copper plating.

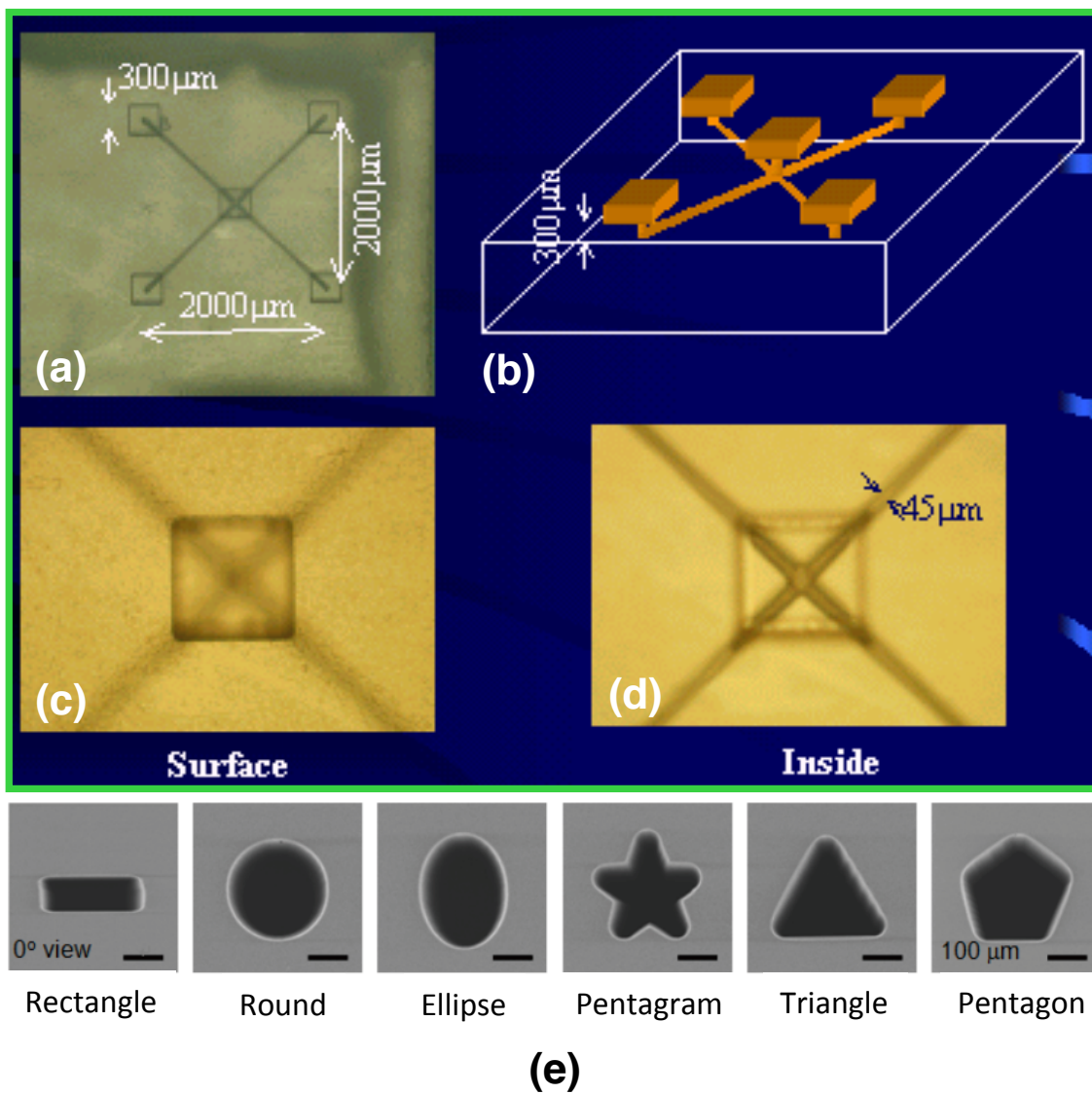


Fig. 5. Fabrication of X-shaped microfluidic channels embedded in photosensitive glass $300\ \mu\text{m}$ below the surface. (a) Overview optical micrograph, (b) 3D schematic illustration of the fabricated structure, and close-up views of the central part when the focus points for observation are set at (c) the surface and (d) the microchannel ($300\ \mu\text{m}$ below the surface). (e) SEM micrographs of designed 3D microfluidic channel cross-sections formed in photosensitive glass using FLAE. Six typical shapes (rectangle, round, elliptical, pentagram, triangle, and pentagon, $250\text{--}280\ \mu\text{m}$ size) were realized [16, 35].

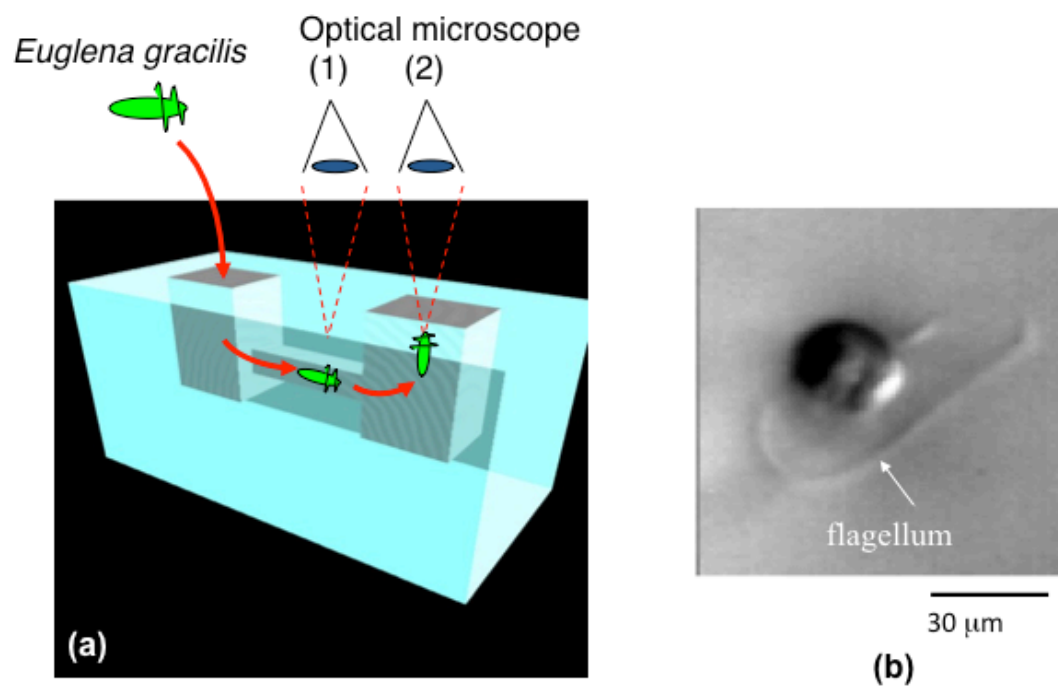


Fig. 6. (a) 3D schematic illustration of nanoaquarium used to observe the motion of *Euglena gracilis*. (b) Optical micrograph of the front view of *Euglena gracilis* swimming in 3D glass microfluidics device fabricated using FLAE [24].

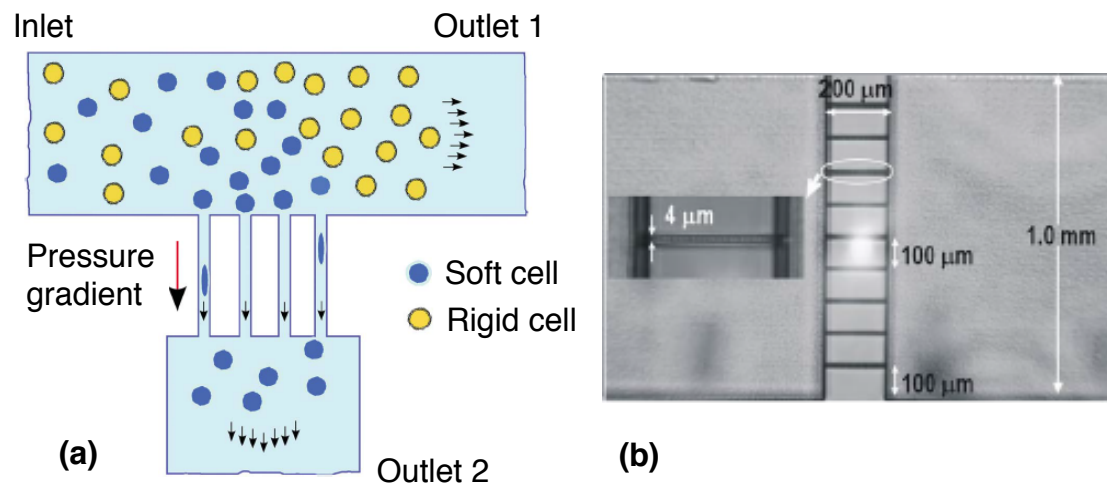


Fig. 7. (a) Schematic illustration of the working mechanism of a 3D cell separator biochip. (b) Top-view optical micrograph of the constriction array in the fabricated biochip [65]. (Reproduced with permission from RSC. ©2012 by the Royal Society of Chemistry.)

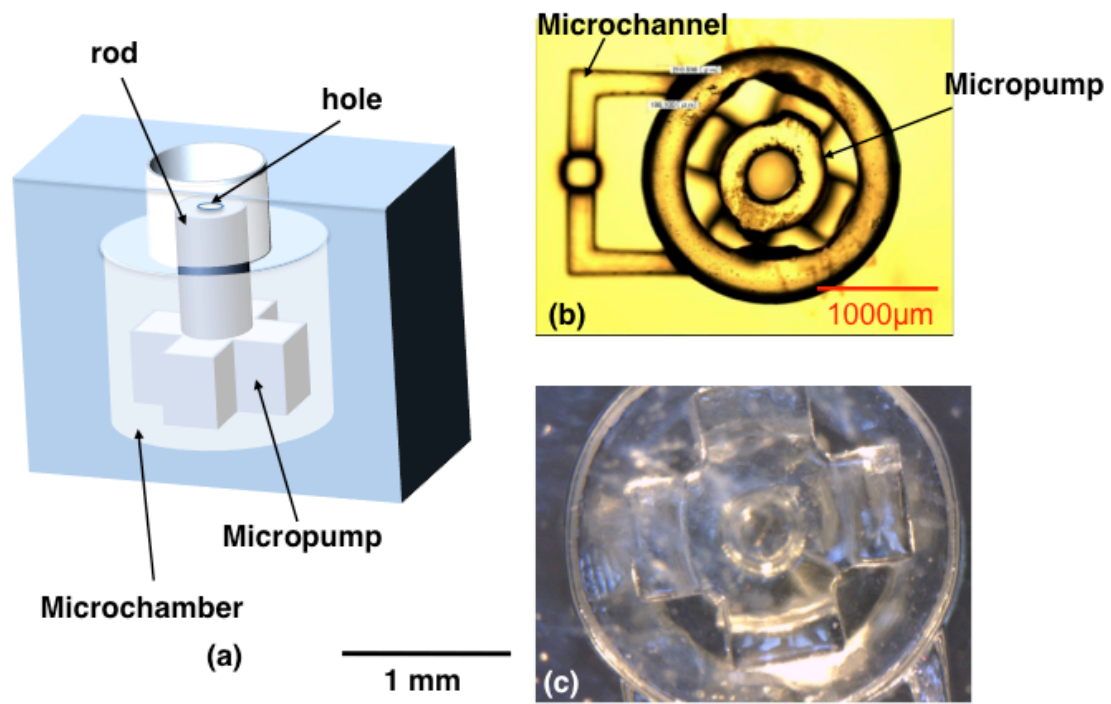


Fig. 8. Micropump fabricated in a 3D microfluidic structure. (a) 3D schematic illustration, (b) overview, and (c) close-up optical micrographs of the fabricated structure [16].

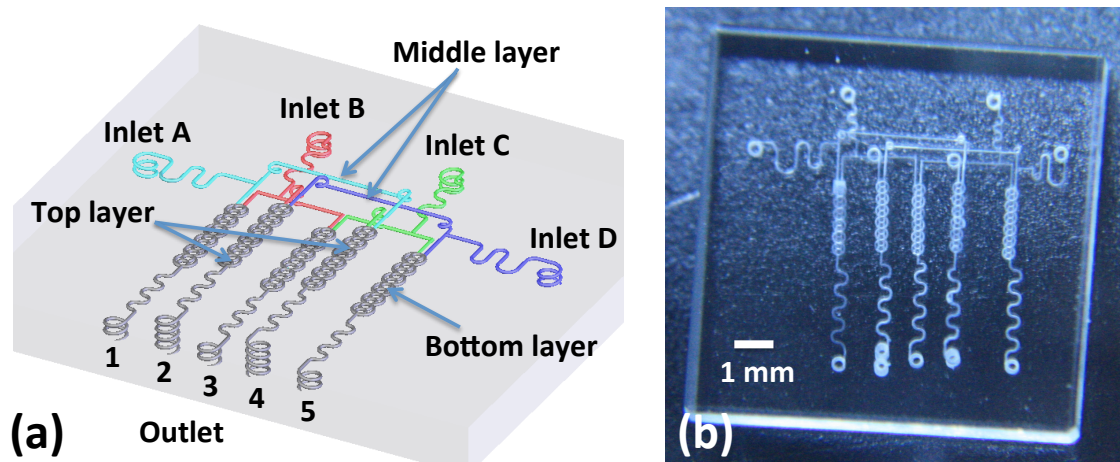


Fig. 9. Multilayered microfluidics system with 3D configuration for simultaneous mixing of different fluids [67]. (courtesy of Y. Li)

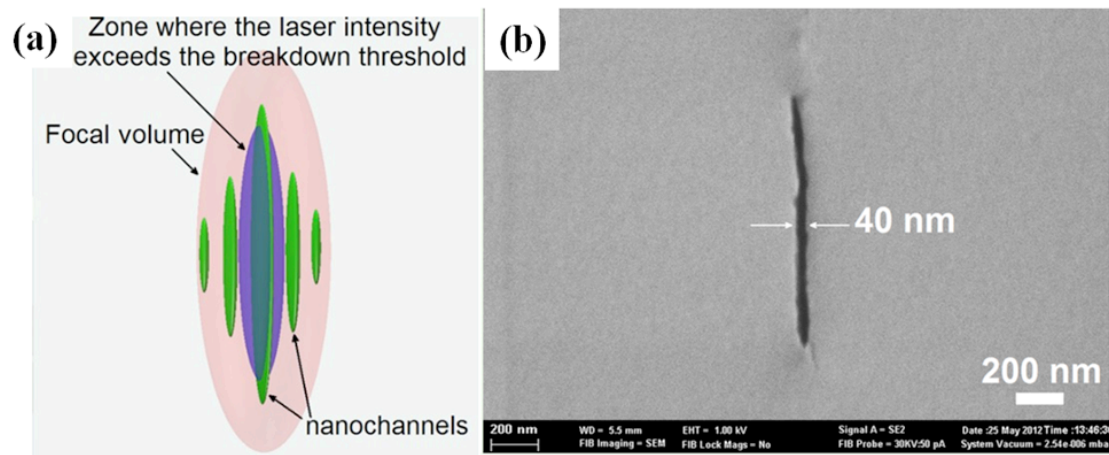


Fig. 10. (a) Schematic diagram of the concept employed to realize the formation of a narrow channel width far beyond the optical diffraction limit. (b) Cross-sectional SEM micrograph of a nanochannel fabricated in porous glass [69].

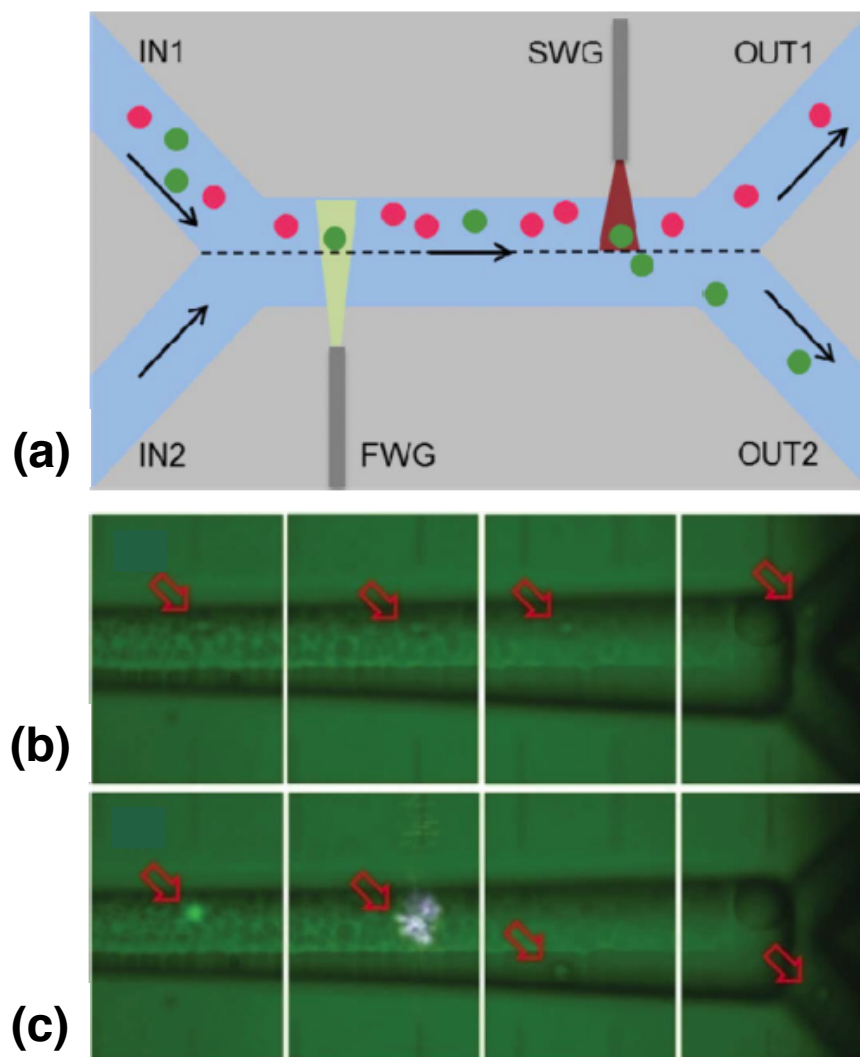


Fig. 11. (a) Principle for cell sorting that utilizes optical forces combined with fluorescence detection. Demonstration of cell sorting when (b) non-fluorescent and (c) fluorescent cells are detected in the optofluidics device [31]. (Reproduced with permission from RSC. ©2012 by the Royal Society of Chemistry.)

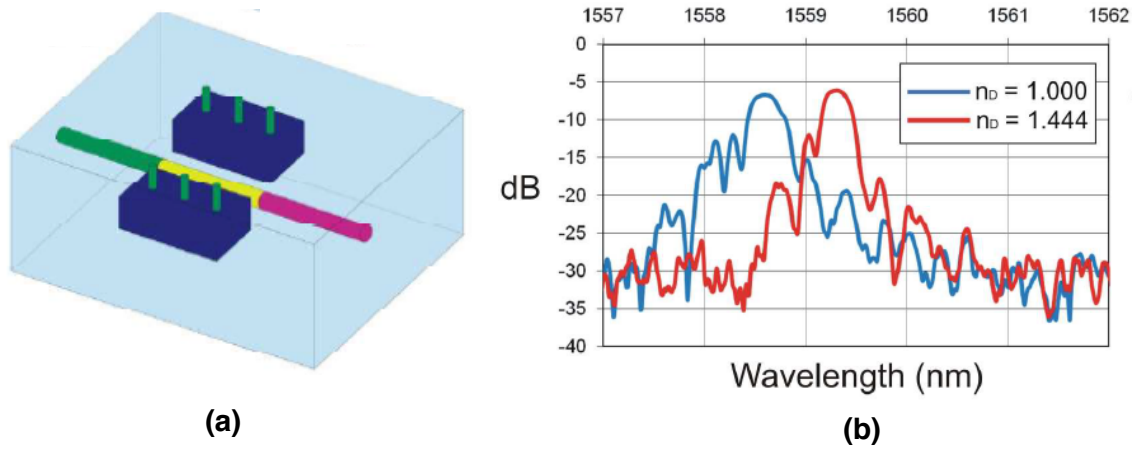


Fig. 12. (a) Schematic geometry of optofluidics sensor based on an evanescent wave, which consists of a straight BGW and double microchannels. (b) Bragg grating reflection spectra (1560 nm grating) for microchannels filled with air ($n_D = 1.000$) and index matching oil ($n_D = 1.444$) [70]. (Reproduced with permission from OSA. ©2009 by the Optical Society of America.)

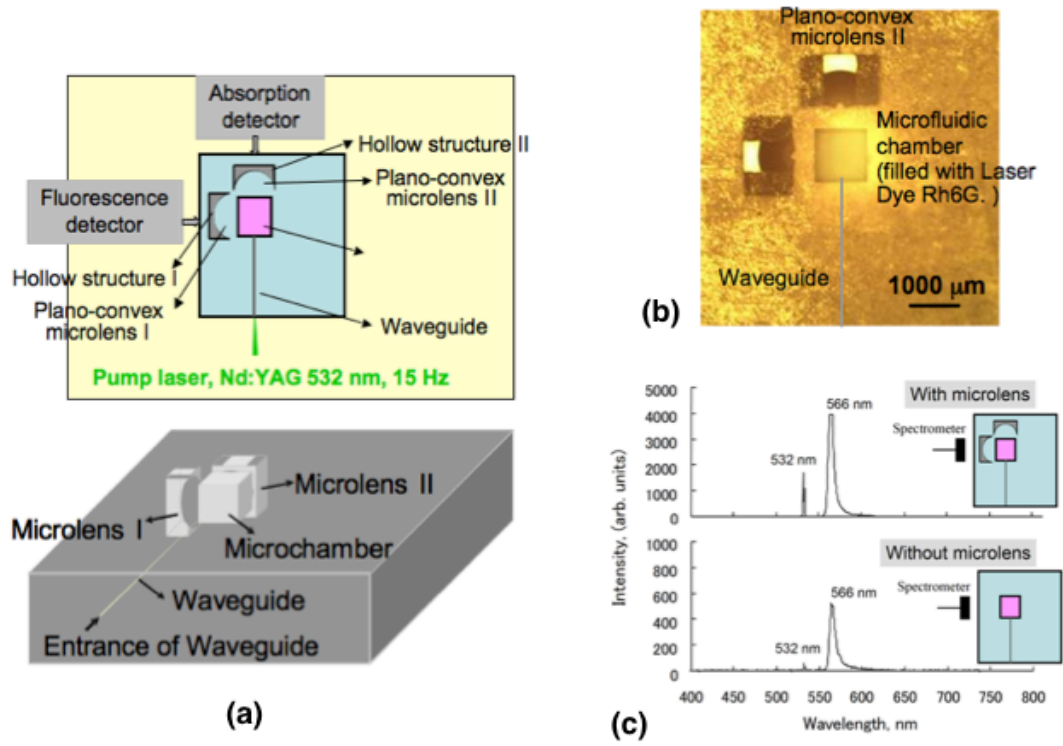


Fig. 13. (a) 2D and 3D schematic configurations and (b) optical micrograph of an optofluidics system in which two plano-convex lenses and an optical waveguide are integrated with a microfluidic chamber in a single glass chip. Note: The solid gray line indicates the invisible waveguide inside the glass. (c) Fluorescence spectra from the laser dye Rh6G pumped by 2ω of a Nd:YAG laser for optofluidics integrated with (upper) and without (lower) plano-convex lenses [40].

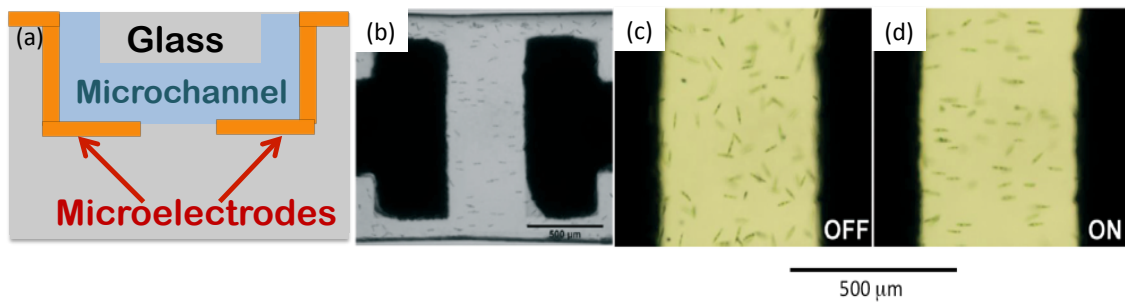


Fig. 14. Electro-orientation of *Euglena* cells in a microfluidic channel. (a) Schematic cross-section of the fabricated electrofluidics device. (b) Overview of electrofluidics system for manipulation of *Euglena* cells, where a pair of electrically isolated microelectrodes are integrated in a microfluidic channel. Movement of *Euglena* cells in the microfluidic channel (c) without and (d) with application of an electric field ($V_{p-p} \sim 28$ V, 0.9 MHz) [17].

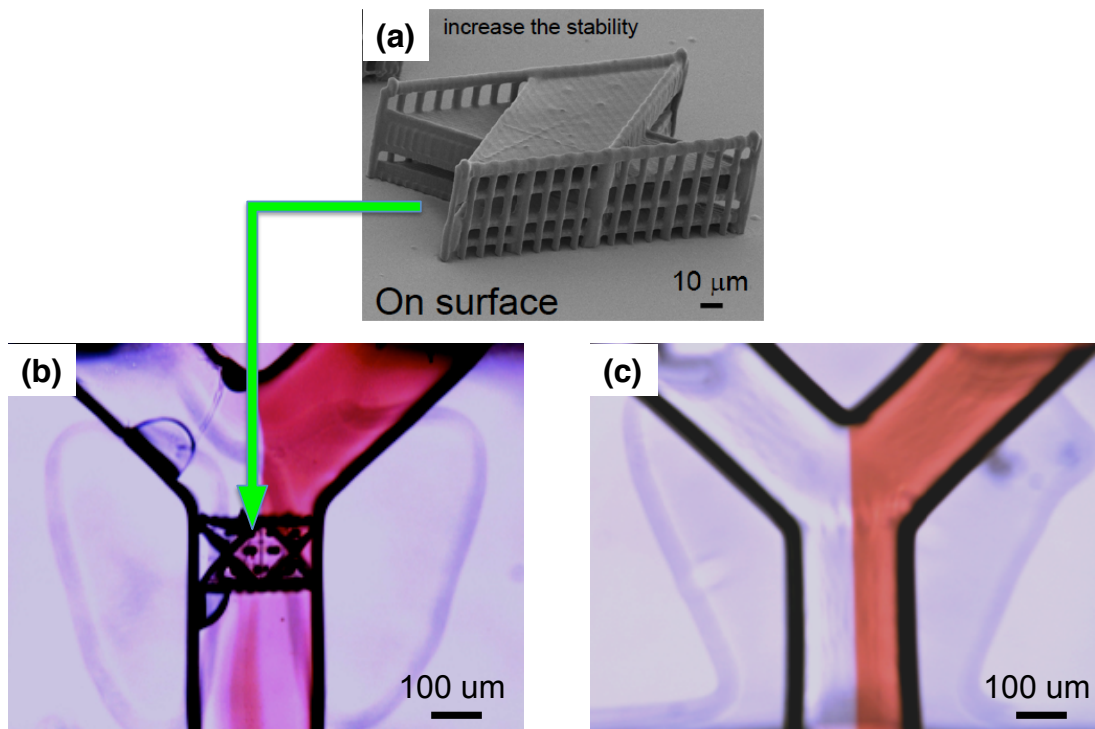


Fig. 15. (a) Microcomponents fabricated by TPP for the efficient mixing of fluids. Comparison of mixing efficiency of Y-shaped microfluidic channels integrated (a) with and (b) without the microcomponent [35].